The impact of self-interacting dark matter on the intrinsic alignments of galaxies

David Harvey [ID],[1]★ Nora Elisa Chisari [ID],[2] Andrew Robertson [ID][3] and Ian G. McCarthy [ID][4]

[1]*Lorentz Institute, Leiden University, Niels Bohrweg 2, Leiden, NL-2333 CA, The Netherlands*
[2]*Institute for Theoretical Physics, Utrecht University, Princetonplein 5, NL-584 CC, The Netherlands*
[3]*Department of Physics, Institute for Computational Cosmology, Durham University, South Road, Durham DH1 3LE, UK*
[4]*Astrophysics Research Institute, Liverpool John Moores University, 146 Brownlow Hill, Liverpool L3 5RF, UK*

ABSTRACT
The formation and evolution of galaxies is known to be sensitive to tidal processes leading to intrinsic correlations between their shapes and orientations. Such correlations can be measured to high significance today, suggesting that cosmological information can be extracted from them. Among the most pressing questions in particle physics and cosmology is the nature of dark matter. If dark matter is self-interacting, it can leave an imprint on galaxy shapes. In this work, we investigate whether self-interactions can produce a long-lasting imprint on intrinsic galaxy shape correlations. We investigate this observable at low redshift ($z <$ 0.4) using a state-of-the-art suite of cosmological hydro-dynamical simulations where the dark matter model is varied. We find that dark matter self-interactions induce a mass-dependent suppression in the intrinsic alignment signal by up to 50 per cent out to tens of mega-parsecs, showing that self-interactions can impact structure outside the very core of clusters. We find evidence that self-interactions have a scale-dependent impact on the intrinsic alignment signal that is sufficiently different from signatures introduced by differing baryonic physics prescriptions, suggesting that it is detectable with upcoming all-sky surveys.

Key words: dark matter; large-scale structure of Universe.

1 INTRODUCTION

Galaxy shapes, both the magnitude of their ellipticity and position angles, are coherently aligned by large-scale tidal fields, sourced by over-densities in the Universe (Croft & Metzler 2000; Heavens, Refregier & Heymans 2000; Lee & Pen 2000; Catelan, Kamionkowski & Blandford 2001; Crittenden et al. 2001; Mackey, White & Kamionkowski 2002; Aubert, Pichon & Colombi 2004; Heymans et al. 2004). Confirmed observationally (Brown et al. 2002; Heymans et al. 2006; Mandelbaum et al. 2006; Hirata et al. 2007; Okumura, Jing & Li 2009; Joachimi et al. 2011; Kirk et al. 2012; Singh, Mandelbaum & More 2015; Singh & Mandelbaum 2016; Johnston et al. 2019), the 'intrinsic alignments' (IA) of galaxies with over-densities are a serious contaminant of weak lensing cosmic shear studies, introducing additional correlations and potentially biasing the inference of cosmological parameters (Hirata & Seljak 2004; Bridle & King 2007; Kirk, Bridle & Schneider 2010; Kirk et al. 2012; Krause, Eifler & Blazek 2016). Frameworks to mitigate the impact of IA on cosmological model inference have been developed, whereby nuisance parameters can be marginalized over (King 2005; Joachimi et al. 2011). This requires insights into the origin of the IA signal, which has resulted in several efforts to analytically model the signal from physical first principles (Catelan et al. 2001). Initial models assumed that the over-densities grow linearly, whereas in practice this is only true down to separations of $\sim 10\,h^{-1}$ Mpc. More recent

efforts have extended this modelling to the quasi-linear regime via perturbative expansions (Blazek, McQuinn & Seljak 2011; Blazek, Vlah & Seljak 2015; Blazek et al. 2019) or effective field theory approaches (Vlah, Chisari & Schmidt 2020a,b), and to the one halo regime via the halo model (Schneider & Bridle 2010; Fortuna et al. 2020). In parallel, progress in hydro-dynamical cosmological simulations, which include complex baryonic physics processes such as feedback from supernova and active galactic nuclei (AGN), has enabled predictions of the IA signal down to $\sim 0.1\,h^{-1}$ Mpc and comparison with observations (Chisari et al. 2015, 2016b; Codis et al. 2015; Tenneti et al. 2015b; Velliscig et al. 2015; Hilbert et al. 2017; Kraljic, Davé & Pichon 2020; Samuroff, Mandelbaum & Blazek 2020; Shi et al. 2020). These simulations help validate and calibrate analytical methods, whilst providing some priors and physical insight into the observed correlations.

While most efforts remain focused on mitigation of IA, they themselves are rich with cosmological information. In particular, alignments are sensitive to baryon acoustic oscillations (Chisari & Dvorkin 2013), an-isotropic primordial non-Gaussianity (Schmidt, Chisari & Dvorkin 2015; Chisari et al. 2016b), primordial gravitational waves (Chisari, Dvorkin & Schmidt 2014; Biagetti & Orlando 2020), and modified gravity (L'Huillier et al. 2017). Different strategies can be useful for extracting this information, including combining multiple shape measurements (Singh & Mandelbaum 2016; Chisari et al. 2016a) or exploiting the mass dependence of the IA signal (Piras et al. 2018). In this paper, we investigate how altering the interacting properties of dark matter may influence the intrinsic alignment of galaxies with overdensities in the Universe.

★ E-mail: davidharvey1986@googlemail.com

Despite the success of the cold and collisionless dark matter paradigm (CDM), we know very little about the particle nature of dark matter, other than its interactions with the Standard Model (protons, neutrons, neutrinos, etc.) must be exceptionally weak. Interestingly, the self-interaction of dark matter is not constrained by the same limits and provides a unique avenue to understand forces within the dark sector without having to assume any coupling to the Standard Model (for a review, see Tulin & Yu 2017). It is thus crucial to constrain the self-interacting dark matter (SIDM) cross-section, most often normalized by its mass: σ_{DM}/m. Such studies often concentrate on the inner profiles of either high- or low-mass haloes (Newman et al. 2013; Harvey et al. 2017, 2018; Read, Walker & Steger 2018; Bondarenko et al. 2020). Recently, it has been suggested that the anticorrelation between the pericentre of the dwarf galaxies and their dark matter central density can be only explained by SIDM (Kaplinghat, Valli & Yu 2019), resulting in a velocity-dependent cross-section (vdSIDM) with $\sigma_{\mathrm{DM}}/m \sim 100\ \mathrm{cm^2\,g^{-1}}$ at the Dwarf Scale, and $\sigma_{\mathrm{DM}}/m \sim 0.1\ \mathrm{cm^2\,g^{-1}}$ at cluster scale (Correa 2020). Indeed, this would be consistent with cluster scale constraints that limit the cross-section to $\sigma_{\mathrm{DM}} < 0.5\ \mathrm{cm^2\,g^{-1}}$ (Harvey et al. 2019; Sagunski et al. 2021).

In this work, we rely on the adapted BAHAMAS-SIDM suite of cosmological simulations to carry out a study of large-scale signatures of SIDM as probed by galaxies around clusters of galaxies in a model where scatterings are late-time and elastic (without any change to the standard ΛCDM primordial power spectrum). Due to the limited mass resolution of the simulations, and because alignments are stronger for higher mass galaxies (Piras et al. 2018), we restrict our study to central galaxies alone. This ensures that we have a complete sample of well-resolved galaxies. We specifically demonstrate that the intrinsic alignments of galaxies are sensitive to the nature of dark matter up to scales of several h^{-1} Mpc.

This paper is set out as follows: In Section 2, we outline the cosmological simulations used; in Section 3, we set out the correlation functions; Section 4 shows our results; in Section 5, we discuss our results; and, in Section 6, we conclude. Throughout this paper, we assume a WMAP9 cosmology (Hinshaw et al. 2013) with $\Omega_{\mathrm{M}} = 0.2793$, $\Omega_{\mathrm{B}} = 0.0463$, $\Omega_{\Lambda} = 0.7207$, $\sigma_8 = 0.812$, $n_{\mathrm{s}} = 0.972$, and $h = 0.700$.

2 COSMOLOGICAL SIMULATIONS OF SIDM

The suite of simulations employed here (BAHAMAS-SIDM) are those laid out in Robertson et al. (2019) and we briefly summarize their properties here. Specifically, BAHAMAS-SIDM was produced by including an implementation of dark matter scattering (SIDM) within the BAryons And HAloes of MAssive Systems (BAHAMAS) model of McCarthy et al. (2017, 2018). The original BAHAMAS suite of simulations includes a number of cosmological hydrodynamical simulations run with the {\sc TreePM-SPH} code GADGET3 (Springel 2005). BAHAMAS includes subgrid physics originally developed for the OWLS project (Schaye et al. 2010) for processes that are not directly resolved in the simulations, including radiative-cooling (Wiersma, Schaye & Smith 2009a), stellar evolution and chemodynamics (Wiersma et al. 2009b), star formation (Schaye & Dalla Vecchia 2008), and stellar and AGN feedback (Dalla Vecchia & Schaye 2008; Booth & Schaye 2009).

The BAHAMAS runs accurately reproduce the local galaxy stellar mass function and the gas mass fractions of galaxy groups/clusters, a result of calibration of the AGN and stellar feedback parameters. However, as shown in McCarthy et al. (2017), the simulations also reproduce a wide range of other observables (e.g. X-ray and tSZ scaling relations, hot gas profiles, evolution of the GSMF, QSO luminosity functions, etc.) without any explicit calibration to do so.

For BAHAMAS-SIDM, the parameters dictating the efficiencies of stellar and AGN feedback were left unchanged from their calibrated values in BAHAMAS. Furthermore, like BAHAMAS, the BAHAMAS-SIDM runs of Robertson et al. (2019) were carried out in large periodic boxes whose side measures $400\ h^{-1}$ Mpc, and they adopt a Plummer-equivalent softening length of $4\ h^{-1}$ kpc (physical) below $z = 3$. Given that the aim of this study is to measure the impact of SIDM on the intrinsic alignments of galaxies out to tens of mega-parsecs, the BAHAMAS simulations provides the ideal volume and resolution to garner sufficient statistics.

We obtain IA predictions from the various SIDM models laid out in Robertson et al. (2019) that include (in addition to CDM) three velocity-*independent* cross-sections of $\sigma_{\mathrm{DM}}/m = 0.1$, 0.3, and 1.0 $\mathrm{cm^2\,g^{-1}}$ and one velocity-*dependent* cross-section, where the differential cross-section is defined as

$$\frac{\mathrm{d}\sigma}{\mathrm{d}\Omega} = \frac{\sigma_0}{4\pi \left(1 + \left(\frac{v}{w}\right)^2 \sin^2\left(\frac{\theta}{2}\right)\right)^2}. \tag{1}$$

Here, v is the relative velocity of two interacting particles, σ_0 and w are parameters of the model corresponding to the cross-section at low-velocities (where it becomes velocity independent), and the turnover velocity. Following this, the momentum transfer cross-section is given by the integral over all solid angles, Ω.

We simulate a velocity-*dependent* cross-section with a normalization of $\sigma_0 = 3.04\ \mathrm{cm^2\,g^{-1}}$ and a turnover velocity of $w = 560\ \mathrm{km\,s^{-1}}$, corresponding to the best-fitting model from Kaplinghat, Tulin & Yu (2016) (corresponding to $\sigma_{\mathrm{DM}} \sim 1\ \mathrm{cm^2\,g^{-1}}$ on cluster scales). BAHAMAS-SIDM adopts the same parameters for the subgrid modelling as the original BAHAMAS runs, since they remain unchanged within the sensitivity of the observations (see Discussion for more) (Robertson et al. 2019). These cross-sections span a regime that includes both already excluded and interesting SIDM models. Constraints have limited the cross-section to $\sigma_{\mathrm{DM}} \lesssim 0.5\ \mathrm{cm^2\,g^{-1}}$ (Harvey et al. 2019; Sagunski et al. 2021), with some observations suggesting that dark matter could self-interact at $\sigma_{\mathrm{DM}} \sim 0.1\ \mathrm{cm^2\,g^{-1}}$ on cluster scales (Correa 2020).

We extract snapshots from four redshift slices: $z = \{0., 0.125, 0.250, 0.375\}$. We focus on this redshift range motivated by significant detections of the alignment signal in low-redshift observations (e.g. Singh et al. 2015). We identify haloes and subhaloes within the simulation box using the SUBFIND algorithm (Springel et al. 2001) and extract all galaxies that have a stellar mass $M^* > 10^{10}\mathrm{M}_\odot\,h^{-1}$. The entire sample of galaxies is referred to as the 'D' sample.

Intrinsic alignments are known to be mass-dependent, with higher mass galaxies exhibiting stronger alignment trends (van Uitert & Joachimi 2017; Piras et al. 2018). We hence hypothesize that, if an impact from dark matter self-interactions is present in the alignment statistics, it will be more prominent for the shapes of centrals. This is indeed verified in our results, and we refer to the sample of centrals from the simulations in what follows as the 'S' sample. Thus, we focus on describing the alignments of the galaxies in S and around density tracers D for the rest of the manuscript. Notice that due to the limitations imposed by a fixed mass resolution, the galaxy samples vary slightly from one simulation run to the other. This is caused by the suppression of the mass function as a result of the self-interactions.
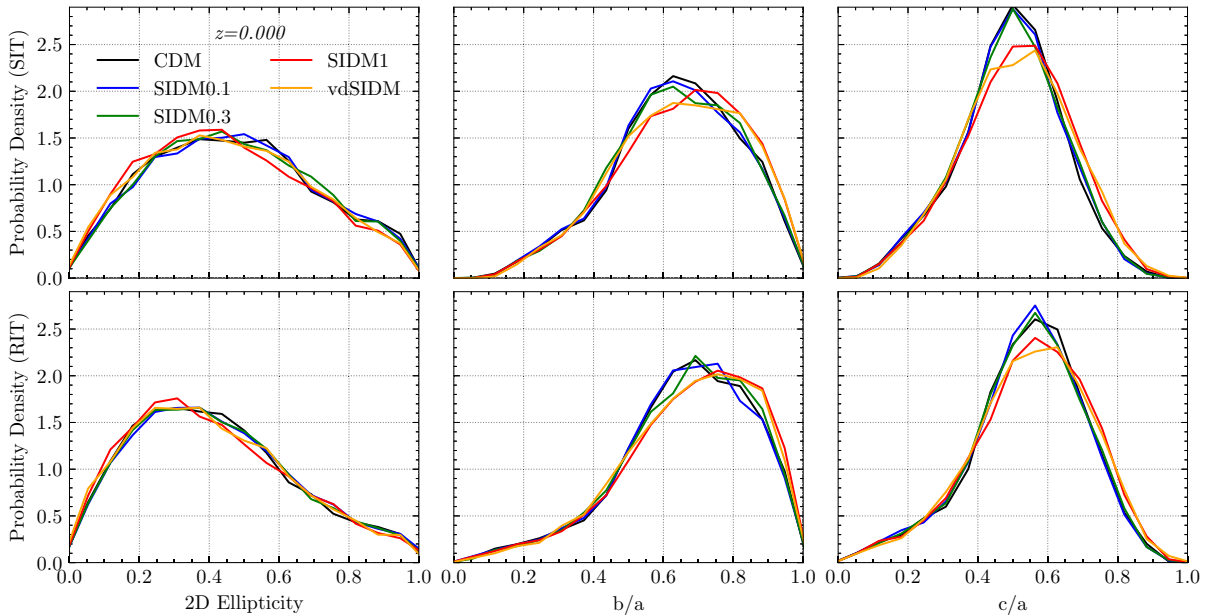
Figure 1. The total distribution of 2D and 3D shapes integrated for $z = 0$, for the simple inertia tensor (SIT, top row) and the reduced inertia tensor (RIT, bottom row). Each colour represents a different dark matter model where we show CDM (black), $\sigma_{\rm DM}/m = 0.1$ (blue), 0.3 (green), and 1.0 cm^2 g^{-1} (red), and vdSIDM (yellow). All shapes are measured within the fiducial radius of 100 physical kpc and using equation (2).

2.1 Shape measurement

We calculate the shape of a galaxy via its inertia tensor,

$$I_{ij} = \frac{\sum_n x_{i,n} x_{j,n} w_n}{\sum w_n}, \qquad (2)$$

where $(x_{i,n}, x_{j,n})$ are the coordinates of the particle and w_n is the weight of particle n. Intrinsic alignments of low-redshift galaxies have been shown to be sensitive to the shape measurement method both in simulations (Chisari et al. 2015; Velliscig et al. 2015; Tenneti et al. 2015b) and in observations (Singh & Mandelbaum 2016; Georgiou et al. 2019a,b). There is evidence for the outskirts of galaxies to be more aligned with each other than their inner regions, a fact that can potentially be exploited for cosmological purposes (Chisari et al. 2016a). To mimic such an effect, we adopt two different weighting schemes in equation (2): simple (SIT) or reduced (RIT). For the SIT, w_n is simply the mass of the particle, m_n (i.e $w_n = m_n$), and for the RIT, it includes the inverse square of the projected distance the particle is from the centre of the halo, (i.e. $w_n = m_n/r_n^2$).

To measure the shapes of the central galaxies, we carry out an iterative process whereby we calculate the moment of inertia of all particles within some given radius of the galaxy centre (and hence the ellipticity). We then re-calculate the moment inertia except now all particles within an elliptical radius defined by the previous iteration estimate of the shape, keeping the area of the ellipse constant (defined by the radius of the initial circle). We continue this iterative process until the shape estimated by two consecutive iterations are within 1 per cent of one another. We initialize this process assuming an ellipticity of zero. Throughout the manuscript we measure the shape of each galaxy within a physical distance of 100 kpc, unless otherwise stated. However, based on the observational evidence for scale dependence of IA measurements quoted above, we also perform a second measurement with SIT shapes within 30 physical kpc. We have verified that the alignments of galaxies in sample S are indeed weaker if measured at this scale.

We calculate two different inertia tensors: one three-dimensional tensor and a projected two-dimensional tensor. The projected inertia tensor can be more directly compared to observed galaxy shapes in photometric surveys, but accessing the three-dimensional information from the simulation allows us to investigate the impact of SIDM in IA to higher significance. We then denote the eigenvalues of each tensor as a^2, b^2 (and c^2), where $a^2 > b^2 > c^2$, each with a corresponding eigenvector defining its direction. We calculate the position angle of the major-axis, a, from its eigenvector and denote this as θ. The two-dimensional ellipticity of a galaxy is defined as

$$e_{+,\times} = \frac{a^2 - b^2}{a^2 + b^2}[\cos(2\theta), \sin(2\theta)]. \qquad (3)$$

The total 2D ellipticity of the galaxy is thus defined as $e = (a^2 - b^2)/(a^2 + b^2)$.

Fig. 1 shows the distribution of projected 2D ellipticities (left-hand column), and 3D shapes with the ratios between the second-largest axis and the largest axis (semimajor, middle column) and smallest axis (semiminor) and the semimajor axis (right-hand column) for the four different dark matter models (varying colours). The top row shows the SIT and the bottom row, the RIT. All the curves in this plot correspond to shape measurements taken within 100 physical kpc. We refer results for shapes starting from 30 physical kpc in Section 4.4. We note that the distributions may seem immediately broader than what is observed in the literature; however, this is due to the choice of ellipticity in equation (3). Often $|e| = (a - b)/(a + b)$ is chosen, resulting in a narrower distribution.

RIT shapes result in higher values for the 3D axis ratios. This is expected, since the RIT measurement tends to circularize them. A similar effect can be seen in the 2D shapes, where RIT results in lower values of e. An increasing value of SIDM cross-section results in further circularization of the shapes. This results agrees with previous studies looking at the shape of dark matter haloes in SIDM cosmologies (Brinckmann et al. 2018; Robertson et al. 2019). The velocity-dependent model yields shapes with a distribution that

is very similar to the SIDM1 model, where $\sigma_{DM} = 1.0$ cm^2 g^{-1}. This is expected since the effective mass of the sample is $\sim 10^{14}$M$_\odot$ and at this halo mass $\sigma_{DM}(v = 500$ km s$^{-1}) \sim 1.0$ cm^2 g^{-1} (Robertson et al. 2019).

A priori, it is impossible to predict the impact of SIDM on IA from Fig. 1 alone. In principle, rounder shapes could lead to either increasing the noise in the alignment signal or to suppressing it, or both. Section 3 introduces the estimators we adopt for investigating the degree of *correlated* impact of SIDM on central galaxy alignments with the large-scale structure.

3 CORRELATION FUNCTIONS

We calculate the correlation between the shape of central galaxies S, with the positions of all density tracers, i.e galaxies D, and the correlation between the position of centrals with the positions of all galaxies. For normalization purposes, we define a sample of randomly distributed points in the simulation box as R_S. This has the same abundance as the sample with galaxy shapes. Analogously, randomly distributed density tracers are labelled R_D.

In a cosmological simulation, availability of three-dimensional shapes for galaxies allows one to define a three-dimensional alignment correlation function as

$$\eta_e(r) = \langle |\hat{r} \cdot \hat{u}(x + r)|^2 \rangle - 1/3, \tag{4}$$

where the hats correspond to unit vectors, u is the direction of the major-axis of a galaxy at position x, and r is the co-moving separation between galaxies, averaged over all galaxy-central pairs with separation r. A positive correlation corresponds to the major-axis pointing parallel to the three-dimensional distance vector separating the two points.

For the projected shapes, we refer to the tangential component of the ellipticity as S_+ and to the cross-component as $S_\times$ (equation 3). We define an estimator for the real-space, normalized correlation function of galaxy shapes and density tracers as

$$\xi_{g+}(r_p, \Pi) = \frac{S_+ D}{R_S R_D}. \tag{5}$$

This is a function of projected co-moving separation, r_p, and line-of-sight co-moving separation, Π, where

$$S_+ D = \sum_{(r_p, \Pi)} \frac{e_{+,j}}{2\mathcal{R}}. \tag{6}$$

Here, $\mathcal{R}$ represents the responsivity of a shape to gravitational shear (Bernstein & Jarvis 2002), and $\mathcal{R} = 1 - \langle e^2 \rangle$, where e_{+j} is the tangential component of the ellipticity for the jth galaxy and $\langle e^2 \rangle$ is the root mean square per ellipticity component. For completeness, we include this factor here, although we are only concerned with the scale dependence of intrinsic alignment correlations. The responsivity factor is only relevant in studies focusing on mitigation of IA in weak lensing cosmology.

We integrate over all line-of-sight bins to get the projected shape–position correlation function, w_{g+}:

$$w_{g+} = \int_{-\Pi_{max}}^{+\Pi_{max}} d\Pi \, \xi_{g+}(r_p, \Pi), \tag{7}$$

and similarly for $w_{g\times}$. We choose our projection length to be $\Pi_{max} = 100 \, h^{-1}$ Mpc. Mandelbaum et al. (2006) and Hirata et al. (2007) found that integrating beyond $60 \, h^{-1}$ Mpc had no impact on the intrinsic alignment signal. Most of the IA signal is localized in narrow line-of-sight bins due to its physical origin (versus the integrated nature of the gravitational lensing effect). In order to obtain
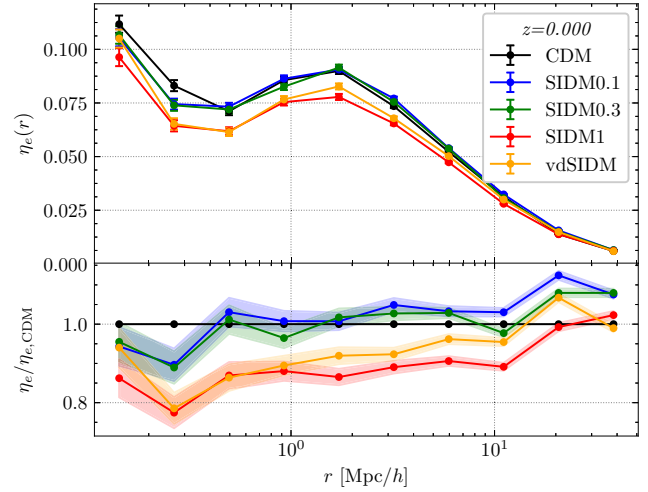
Figure 2. Three-dimensional correlation between the direction of major axes of central galaxies and the separation vector towards all other galaxies at $z = 0$. Top panel: We show the absolute three-dimensional correlation (equation 4) for each dark matter model. Bottom panel: We show the ratio of the correlation in each model to the CDM case.

an estimate of the error in the intrinsic alignment signal, $\sigma_{wg+SIDM}$, we jackknife the sample of galaxies by splitting each volume in to nine subvolumes. This acts to provide us a signal-to-noise estimate for each dark matter model. As such we show the signal-to-noise ratio relative to a benchmark value (for instance CDM or $z = 0$) in each plot, i.e. $(w_{g+,SIDM} - w_{g+,CDM})/\sigma_{wg+,SIDM}$.

Since w_{g+} is sensitive to the clustering bias of galaxies as well as their IA bias, we complement this measurement by also obtaining the clustering (position–position) correlation function for the cross-correlation of S and D. This allows us to determine whether any impact of SIDM observed in w_{g+} might be a consequence of a change in the clustering properties of the samples. The projected clustering correlation, w_{gg}, is given by

$$w_{gg} = \int_{-\Pi_{max}}^{+\Pi_{max}} d\Pi \, \xi_{gg}(r_p, \Pi), \tag{8}$$

where

$$\xi_{gg}(r_p, \Pi) = \frac{SD}{R_S R_D} - 1. \tag{9}$$

Unless explicitly exploring the redshift dependence of our results (discussed in Section 4.2), all the figures presented are the results of the redshift stated in the legend of each caption.

4 RESULTS

4.1 Sensitivity of IA to SIDM

We begin by examining the three-dimensional correlation function (cf. equation 4) to see if self-interactions have an impact on the alignment of central galaxies around density tracers. The top panel of Fig. 2 shows the three-dimensional alignment signal for the five different dark matter models. We show in the bottom panel of Fig. 2 the alignment signal in the interacting dark matter models relative to the CDM value. Self-interactions yield a significant suppression in the IA signal that persists to large scales. This suppression is more prominent for increasing cross-sections and can be observed between central-galaxy pairs separated by distances greater than 100 kpc.
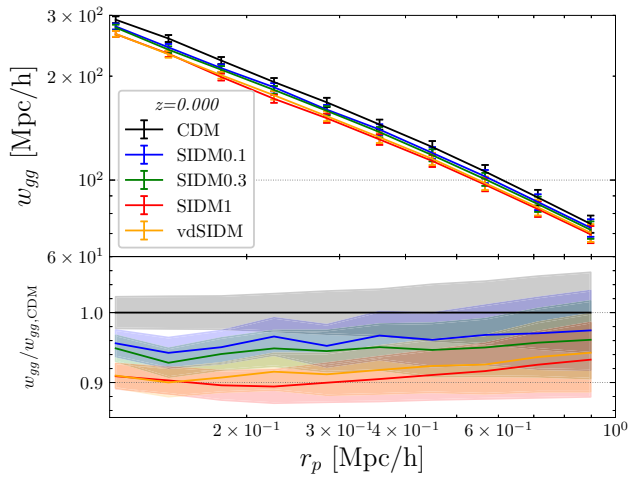
Figure 3. Autocorrelation of galaxy clustering for samples D out to $1\,\mathrm{Mpc}\,h^{-1}$. Top panel: We show the clustering correlation of all galaxies for different dark matter models. Bottom panel: We show the ratio of the projected correlation for each model relative to the CDM model.

These results are consistent with the circularization of the shapes produced by SIDM in Fig. 1. Such a process would introduce random noise in the orientation of the galactic major axes and suppress the alignment correlation. This frequently used statistic only takes into account the galaxy orientations, without considering whether the dark matter model can induce correlated changes in galaxy axis ratios. This is remedied when considering the projected shape correlation of equation (7).

We show the projected galaxy autocorrelation of the 'D' sample (equation 8) in Fig. 3 and the analogous IA signal (equation 7) in Fig. 4 for the five different dark matter models. The bottom panel of Fig. 3 corresponds to the ratio between the clustering correlation in the self-interacting models and the CDM case. We note that this signal is calculated to only $1\,\mathrm{Mpc}\,h^{-1}$. The clustering signal is suppressed at small scales relative to CDM, although this is limited to no more than 10 per cent and is only significant well within intra-halo scales ($\lesssim 0.4\,h^{-1}\,\mathrm{Mpc}$). Since the galaxy samples have not been

cross-matched across simulations, such a change could be driven by intrinsic changes in the galaxy bias or by a selection effect.

The top panels of Fig. 4 show the $w_{g,+}$ and $w_{g,\times}$ correlations of central galaxy shapes with density tracers. The left-hand figure corresponds to SIT shapes, the right-hand figure corresponds to RIT shapes. We test that $w_{g,\times}$ is consistent with null through symmetry and find that the data has a $\chi^2_{\mathrm{red}} = 0.8 \pm 0.4$ (SIT) and 1.1 ± 0.4 (RIT) consistent with 1 for a model where $w_{g,\times} = 0$ for all scales, while there is a significant negative measurement of w_{g+}, which indicates a projected radial alignment of S galaxies around D tracers. Moreover, RIT shapes result in a lower alignment amplitude than SIT shapes. Both results are in qualitative agreement with observational trends (e.g. Singh et al. 2015; Singh & Mandelbaum 2016). The bottom panels of Fig. 4 show the relative difference with respect to CDM. We find that intrinsic alignments are suppressed by dark matter interactions, with the velocity-dependent cross-section exhibiting a suppression of $w_{g+}/w_{g+,\mathrm{CDM}} > 20$ per cent at $r = 0.1\,h^{-1}\,\mathrm{Mpc}$. The suppression of the IA correlation can persist out to $r > 1\,h^{-1}\,\mathrm{Mpc}$ from the cluster centre. The suppression can be interpreted as an overall misalignment of the central galaxy shape with the location of nearby galaxies.

4.2 Redshift and mass dependence

Intrinsic alignment correlations are known to be mass-dependent, with higher mass haloes being subject to stronger alignment in line with a power-law scaling with stellar mass (or luminosity) (Singh et al. 2015; van Uitert & Joachimi 2017; Piras et al. 2018). Although not very well-constrained currently, the redshift dependence of the alignment signal is another observable, which could, in the future, allow for a distinction between different alignment or dark matter models. We explore both scalings in this section. To mitigate possible differences in the alignment signal due to selection effects in the sample of central galaxies, we restrict here to the 4800 most massive haloes in the simulations. (This choice corresponds to the minimum number of centrals of all redshift and dark matter models.)

We investigate the mass dependence of the alignment signal in Fig. 5. We split the sample of haloes into three mass bins: $13.5 < \log(M/M_\odot) < 14.0$, $14.0 < \log(M/M_\odot) < 14.5$, and $14.5 <$
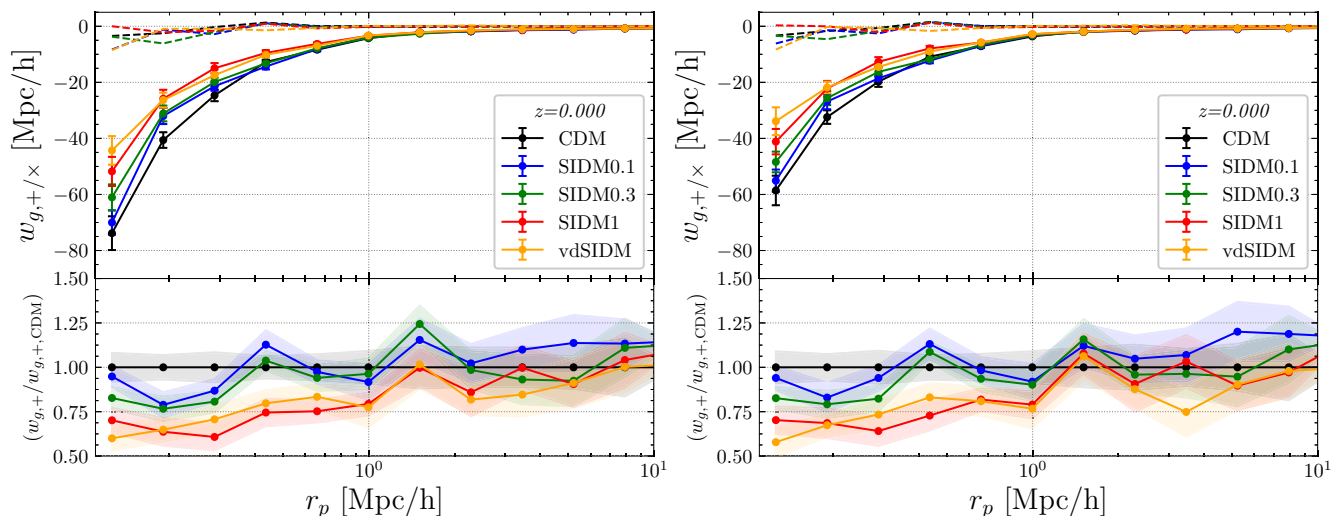
Figure 4. Projected shape–position correlation between galaxies in sample S and sample D for $z = 0$. Left-hand panel: the absolute projected intrinsic alignment correlation for different dark matter models using SIT shapes measured at $r_{\mathrm{meas}} = 100\,\mathrm{kpc}$ and integrated over all redshifts. Both the w_{g+} (solid) and $w_{g\times}$ (dashed) correlations are shown. The bottom panel compares signal relative to CDM. Right-hand panel: analogous results for RIT.
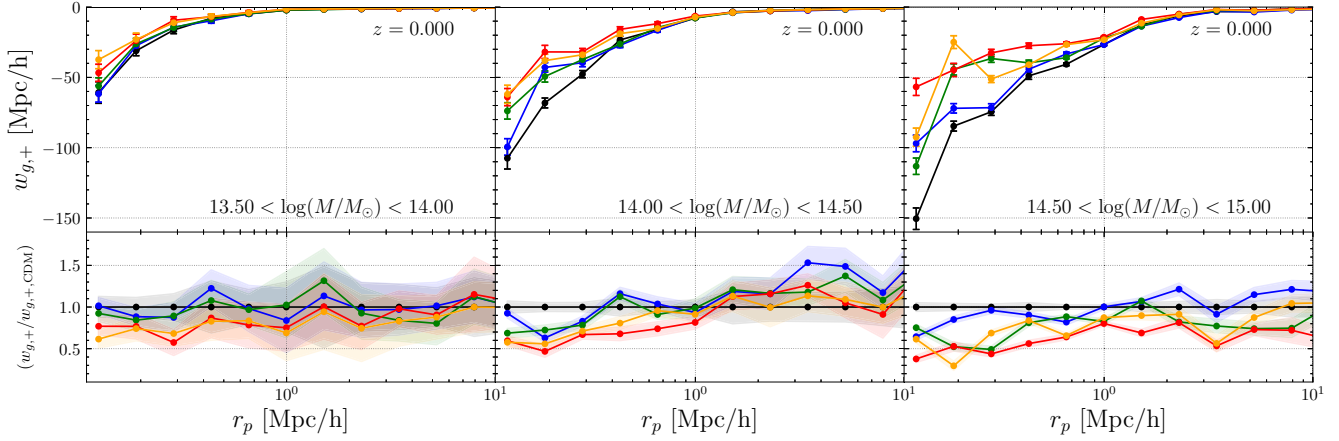
Figure 5. The mass dependence of the intrinsic alignment signal for three mass bins (denoted by the legend in each panel). The top panels show the absolute signal for each dark matter model: CDM (black), $\sigma_{DM}/m = 0.1$ (blue), 0.3 (green), and 1.0 cm^2 g^{-1} (red), and the velocity-dependent cross-section 'vdSIDM' (yellow). The bottom panels show the signal relative to CDM.
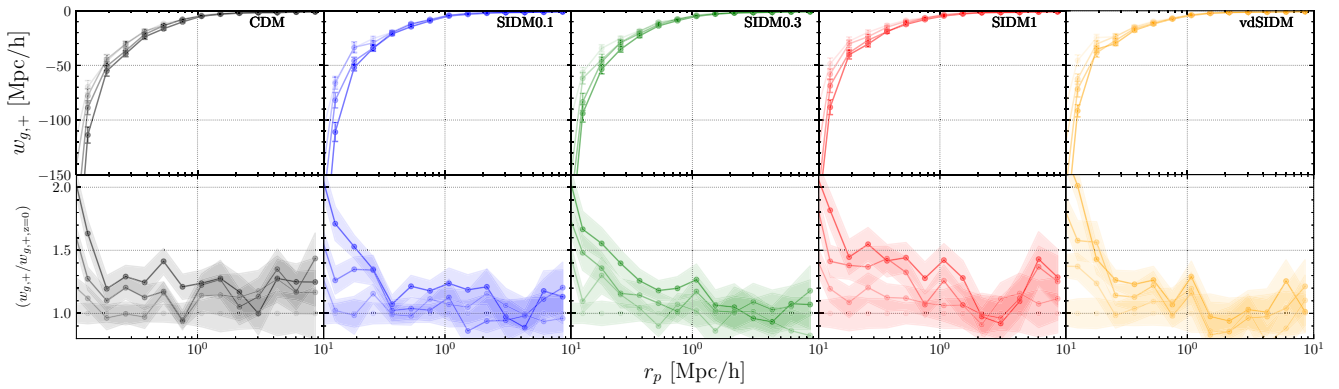
Figure 6. Redshift dependence of each simulation for the 4800 most massive haloes in each redshift slice ($z = 0, 0.125, 0.250, 0.375$, increasingly solid colour). Top panels: the absolute signal for the different dark matter models. Bottom panels: We show the signal relative to $z = 0$.

$\log (M/M_{\odot}) < 15.0$ (left- to right-hand panels) for $z = 0$ and show the absolute signal in the top panels of Fig. 5 and the signal relative to CDM in the bottom panels. We find that the alignment correlation increases with halo mass, and that the mean relative suppression inside 1 Mpc h^{-1} due to the interacting dark matter models also increases with mass, from $w_{\rm SIDM1}/w_{\rm CDM} = 0.85 \pm 0.03$ in the lowest mass bin to $w_{\rm SIDM1}/w_{\rm CDM} = 0.59 \pm 0.03$ in the highest mass bin. However, the highest mass bins suffers from larger variance due to the low number of clusters.

Fig. 6 shows the alignment signal for the four redshift bins studied. We separately analyse each of the five dark matter models (each panel), with the top panel of each showing the absolute signal and the bottom panel the signal relative to $z = 0$. In each case, we show increasing redshift with darker colours for the four redshifts $z = \{0, 0.125, 0.250, 0.375\}$. The top panels show that the alignment signal increases towards higher redshift for all models. This is in contrast with the clustering signal, shown in Appendix A1, which increases towards lower redshifts (reflecting the build-up of structures). This redshift dependence is similar in all models (and between different levels of AGN heating for the CDM), which motivates us to think that this is a selection effect. However, it is over a very small redshift range and will need to be expanded to be explored completely.

4.3 Impact of baryonic physics

Intrinsic alignments are sensitive to the amount of baryonic feedback in hydro-dynamical simulation, representing an uncertainty in this work (van Daalen et al. 2014; Soussana et al. 2020). A change in the AGN heating temperature in the simulations drives changes in the alignment signal similar to those resulting from the interacting dark matter model. To distinguish between these scenarios, we study two further AGN models in the CDM case. These cases include the extreme ends of the allowed AGN heating temperature that still result in a consistent galaxy stellar mass function. They correspond, however, to a very different gas fraction in these large systems, still within observational limits (McCarthy et al. 2018).

We measure the intrinsic alignment signals in these two simulations at two redshift slices and show the results in Fig. 7, where we show $z = 0$ in the left-hand and $z = 0.375$ in the right-hand panels, a grey-shaded region denotes the upper and lower limits of the measured alignment signal, along with the five dark matter models. The bottom panel shows the suppression of the two dark matter models relative to CDM including the uncertainty in the AGN feedback. We find that at $z = 0$, the AGN feedback represents a large uncertainty in the alignment signal, and without further simulations would be difficult to distinguish from SIDM. However, at higher redshifts, the uncertainty introduced by AGN is fractionally less,
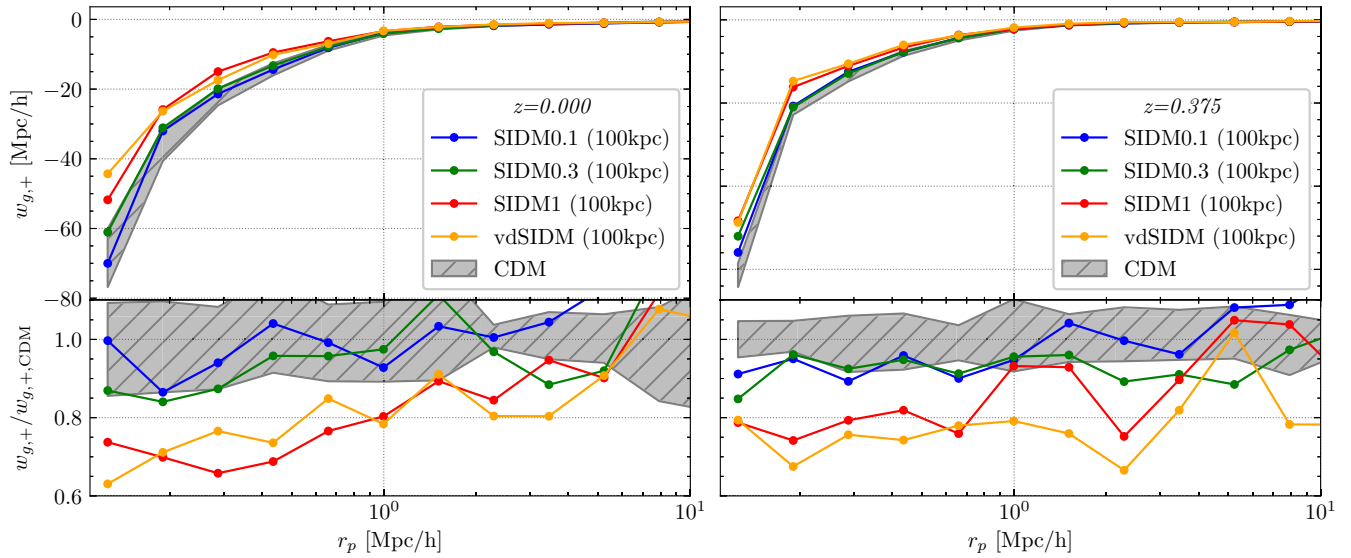
Figure 7. Impact of baryonic feedback on projected alignment statistics for two redshift slices (left-hand panel: $z = 0$ and right-hand panel: $z = 0.375$). Top panels: The shaded region shows the expected uncertainty between two extreme AGN models. We show SIDM0.1 (blue) and SIDM1 (red) for a reference. Bottom panel: comparison of the uncertainty in each dark matter model with the uncertainty in the AGN propagated through.

whilst the SIDM signal remains large. This represents a possible route to disentangling SIDM from CDM.

4.4 Impact of shape measurement method

Throughout our study, we have used the shape of the central galaxy measured at 100 kpc. However, the choice of shape measurement method may probe different regions of the galaxy and hence result in a different IA signal. This was already demonstrated by the differences observed in the alignment signal in the case of SIT and RIT shapes in Fig. 4.

Here, we analyse the IA signal at a second radial scale of the central galaxy. Fig. 8 shows the estimated signal for galaxies measured at the fiducial $r = 100$ kpc and at a (conservative) smallest trusted radii of $r = 30$ kpc (corresponding to a conservative five times the Plummer-equivalent softening scale of $\epsilon = 4\,h^{-1}$ kpc). Although at this scale we again observe a suppression in the IA signal, it is significantly stronger than at 100 kpc. However, we also find that the signal is more sensitive to the choice of AGN model at this scale, and therefore does not necessarily represent an increase in the signal-to-noise ratio.

Nevertheless, the bottom panel shows that the impact of the choice of radial scale is higher in models with increased self-interactions. As a consequence, combining two measurements of galaxy shapes at different scales could yield stronger constraints on the interaction cross-section.

4.5 Power-law fits

Having measured the intrinsic alignment signal in different SIDM cosmologies, we now ask the question of whether it is possible to differentiate between CDM and SIDM in data. Given the uncertainties between observations and simulations, a scale-*independent* change in the intrinsic alignment signal (i.e. a shift in the amplitude) will be difficult to measure; however, a scale-dependent shift will provide a much clearer and more discriminate test.

In order to measure the scale-dependent and independent shifts in the signal, we fit an empirical power-law model to the measured IA
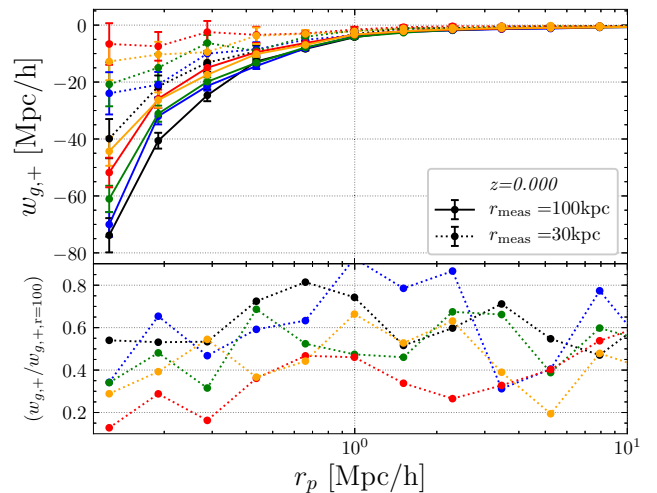

Figure 8. The top panel shows the alignment signal for two different shape measurements: within 30 (dotted) and 100 kpc (solid). As expected, the alignment amplitude is smaller when shapes are measured in the inner region. The bottom panel shows the ratio between the alignment signal with the two shape measurements. This ratio depends on the dark matter interaction model, with more interacting model showing increased differences in alignments with scale.

signals:

$$\log_{10}\left(\frac{w_{g,+}}{\mathrm{Mpc}\,h^{-1}}\right) = \log_{10}\left(\frac{A}{\mathrm{Mpc}\,h^{-1}}\right) + \beta\left(\frac{r_{\mathrm{p}}}{\mathrm{Mpc}\,h^{-1}}\right). \quad (10)$$

where A is the amplitude and β is the power-law index. It has been shown that this is a good description of multiple small-scale alignment statistics (Singh et al. 2015; Georgiou et al. 2019a,b; Fortuna et al. 2020). Any significant dependence of β on the cross-section will be evidence for a scale-dependent shift.

We fit this empirical law to each observation down to a given scale radius. We define this radius by the radius at which the mean reduced χ^2 for the fit with respect to the data is closest to 1. We
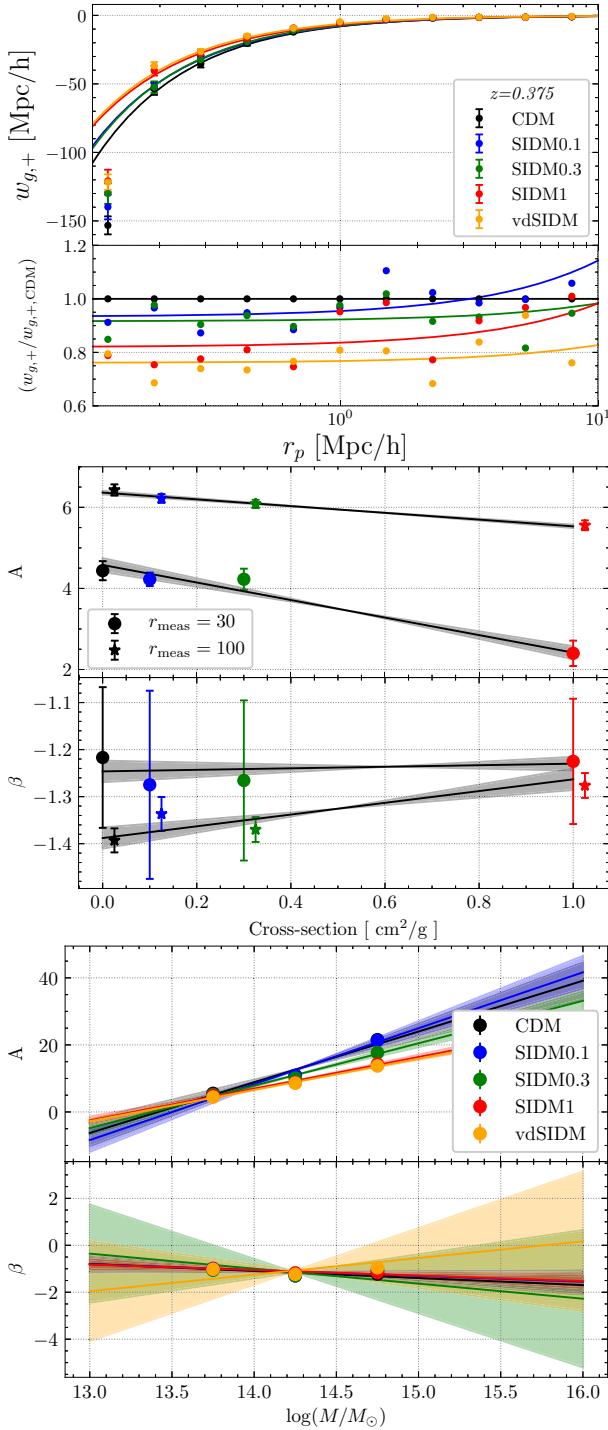
Figure 9. Estimates of the amplitude, A, and power-law index, β, fitted to each IA signal. From the top to bottom: The first panel shows the direct power-law fits to the data (top panel) and the scale dependence of the relative difference to CDM that will be potentially detectable. The middle plot shows the dependence of the power-law fits on cross-section, and the third panel shows the dependence of the power-law fits on mass.

find that the best-fitting scale is at $r = 0.23\ \mathrm{Mpc}\,h^{-1}$. We show the results for the parameter fits in Fig. 9. The left-hand figure shows the direct fit to data of the power law and the relative difference with respect to CDM in the bottom panel. We show the scale dependence of the relative difference for each cross-section in the solid line.

The second panel shows the derived parameters from the fits as a function of cross-section with the top panel showing the shift in the amplitude (scale-independent) and the bottom panel the shift in the slope (scale-dependent). We then fit a linear relation with the interaction cross-section and find

$$A_{30\,\mathrm{kpc}} = (4.56 \pm 0.17) - (2.14 \pm 0.33)\left(\frac{\sigma_{\mathrm{DM}}/m}{\mathrm{cm^2\,g^{-1}}}\right), \tag{11}$$

$$A_{100\,\mathrm{kpc}} = (6.37 \pm 0.05) - (0.84 \pm 0.09)\left(\frac{\sigma_{\mathrm{DM}}/m}{\mathrm{cm^2\,g^{-1}}}\right), \tag{12}$$

$$\beta_{30\,\mathrm{kpc}} = (-1.25 \pm 0.02) + (0.03 \pm 0.03)\left(\frac{\sigma_{\mathrm{DM}}/m}{\mathrm{cm^2\,g^{-1}}}\right), \tag{13}$$

$$\beta_{100\,\mathrm{kpc}} = (-1.39 \pm 0.02) + (0.13 \pm 0.04)\left(\frac{\sigma_{\mathrm{DM}}/m}{\mathrm{cm^2\,g^{-1}}}\right). \tag{14}$$

We find that there is a strong, scale-independent shift with cross-section, and when the shape of a galaxy is measured out to 100 kpc, then we find evidence for a scale-dependent shift at 3σ confidence. This provides promising evidence that intrinsic alignments can be used to constrain SIDM.

We study the mass dependence of each relation since we know that in the CDM cases IA is dependent on halo mass. To do this we measure the IA power-law fits and then fit a linear (in log mass) trend. The bottom panel of Fig. 9 shows the mass dependence of the IA signal with the different dark matter models. We find significant evidence that an increase in halo mass shifts the amplitude of the power-law but not the slope. However, we do find that the mass dependence of the amplitude shift is clearly dependent on the cross-section, with strong self-interactions dampening the impact of increased halo mass.

We conclude that the scale-dependent and mass dependence of the amplitude may provide a pathway to constraining SIDM with IA. For example, by constraining a simulation calibrated β, it would be possible to compare this to observed values. Alternatively, it may be possible to normalize any observable to the high-mass bin and then measure the mass dependence of the amplitude and compare that to what is expected from simulations of CDM.

4.6 Non-linear alignment model

Here we have fitted an empirical power-law model. However, often a more physically motivated non-linear alignment (NLA) model is used to estimate the amplitude of the IA signal (Blazek et al. 2019; Johnston et al. 2019). We attempt here to fit the amplitude of the NLA to our data in the regime where it is suitable. We define 'suitable' as where the reduced χ^2 of the NLA model is closest to one for the CDM model. We find this to be for scales $r_{\mathrm{p}} > 0.6\ \mathrm{Mpc}\,h^{-1}$ ($\chi^2_{\mathrm{red}} = 1.03$). We then determine the reduced χ^2 for the three other other models and find that they deviate from the NLA with increasing cross-section (for scales $r_{\mathrm{p}} > 0.6\ \mathrm{Mpc}\,h^{-1}$). We find that the three cross-sections, $\sigma_{\mathrm{DM}}/m = 0.1, 0.3$, and 1.0, have a $\chi^2_{\mathrm{red}} = 1.3, 1.5,$ and 1.8, respectively. Although SIDM deviates from the NLA model, we find that it would be difficult to use this as a method to constrain SIDM.

5 DISCUSSION

We have presented the impact of dark matter self-interactions on the intrinsic alignment of galaxies with centrals. We have found that dark matter self-interactions significantly suppress the amplitude of the intrinsic alignment signal and show how self-interactions can impact structure at the mega-parsec scale. We also present evidence for a scale-dependent shift, with self-interactions modifying the power-

law index. This behaviour will provide an important feature if we are to constrain SIDM in this way.

If we compare our results to the Horizon-AGN simulations (Chisari et al. 2017), we find that the measured three-dimensional correlation function $\eta(r)$ is similar in trend to that of the satellite–satellite plus central–satellite correlation function, with the increased correlation at ~ 1 Mpc h^{-1}. This is interesting given that our sample contains only centrals. We hypothesize that this is due to the two-halo term of mis-identified centrals in the sample that are in fact satellites and that are large enough to enter the sample. Interestingly, Chisari et al. (2016b) found that the projected intrinsic alignment signal decreased with redshift for a luminosity limited sample, whereas here we find the opposite trend, albeit at lower redshift. On the contrary, Tenneti et al. (2015a) found weak evolution of the projected alignment signal with redshift (in he range $0 < z < 1$) for a mass-limited sample in the MassiveBlack-II simulation. In general, a direct comparison of BAHAMAS-SIDM with these cosmological numerical simulations is difficult, given the differences in halo mass and resolution. Indeed, we carried out a verification on the clustering signal to check that this was growing with redshift and find this agrees with the literature. This dependence should be examined in future to see if it is real. However, independent of whether the CDM signal increases or decreases with redshift, we would expect the observed *relative* suppression due to SIDM to be larger at lower redshift since the rate of self-interactions is constant in time (Robertson et al. 2015).

We note that the AGN and stellar feedback parameters for the BAHAMAS-SIDM simulations were not re-calibrated from the fiducial values used with CDM. This was because the changes to the calibration metrics (such as the stellar mass function) were smaller than the errors on the observational data that was being calibrated to. However, we find that the number of central galaxies that are above required threshold to get a robust shape is dependent on the cross-section of dark matter. For example, the three CDM runs (fiducial, high, and low AGN reheating) have 23 339, 21 689, and 24 927 centrals, respectively. The four SIDM runs, SIDM0.1, SIDM0.3, SIDM1, and vdSIDM have 22 764, 22 784, 22 793, and 22 883, respectively. We see that the number of galaxies in each SIDM run lies within the range of galaxies for the three AGN runs. As such the simulations do not require re-calibration. However, in the future, as the stellar mass function becomes better constrained, hydro-dynamical SIDM simulations with the objective of precise cosmology may need to be re-calibrated in order to be consistent with observations. Moreover, we have not explored any cosmological degeneracy and whether altering the cosmological parameters can mimic the impact of self-interactions. This is something that would need to be explored in future work.

6 CONCLUSIONS

We have used a modified version of BAHAMAS, BAHAMAS-SIDM, to measure the impact of dark matter self-interactions of the intrinsic alignment of galaxies. We correlate all galaxies with the position and shape of central galaxies and measure the three-dimensional alignment and the alignment from the projected two-dimensional shape. We find the following:

(i) Dark matter self-interactions induce a suppression of the alignment signal of central galaxies. This can be as high as 50 per cent depending on redshift, mass range, and dark matter model.

(ii) Degeneracies with AGN feedback can complicate interpretation of SIDM for low cross-sections, however we find that the range of

AGN heating that is compatible with observations is distinguishable from $\sigma_{DM} = 0.1$ cm^2 g^{-1}.

(iii) We fit empirical power-law models down to $r_{cut} > 0.23$ Mpc h^{-1}, where the χ^2_{red} is closest to 1. We find a strong scaling of the alignment amplitude and power-law index with the SIDM cross-section. However, the mass only impacts the amplitude and not the power-law index, suggesting a possible route to disentangling the CDM signal from the SIDM one.

To summarize, we have shown that self-interactions suppresses the intrinsic alignment signal of galaxies with even small interactions impacting the signal out to $\sim$Mpc scales. We show that the scale dependence of the suppression is potentially detectable with upcoming surveys such as *Euclid* (Laureijs et al. 2011) or the Vera C. Rubin Observatory (Ivezić et al. 2019). However, to determine the redshift dependence and to categorize the scale dependence more precisely, larger simulations are required in order to garner better statistics, plus more observationally matched products such as colours and magnitudes are important if these are to be compared to data. However, it is clear that large-scale surveys can have a part to play in the quest to unveil the mystery of dark matter via intrinsic alignments.

## DATA AVAILABILITY

All data are private but available upon request.

REFERENCES

Aubert D., Pichon C., Colombi S., 2004, MNRAS, 352, 376
Bernstein G. M., Jarvis M., 2002, AJ, 123, 583
Biagetti M., Orlando G., 2020, J. Cosmol. Astropart. Phys., 2020, 005
Blazek J., McQuinn M., Seljak U., 2011, J. Cosmol. Astropart. Phys., 2011, 010
Blazek J., Vlah Z., Seljak U., 2015, J. Cosmol. Astropart. Phys., 2015, 015
Blazek J. A., MacCrann N., Troxel M. A., Fang X., 2019, Phys. Rev. D, 100, 103506
Bondarenko K., Sokolenko A., Boyarsky A., Robertson A., Harvey D., Revaz Y., 2020, J. Cosmol. Astropart. Phys., 01, 043
Booth C. M., Schaye J., 2009, MNRAS, 398, 53
Bridle S., King L., 2007, New J. Phys., 9, 444
Brinckmann T., Zavala J., Rapetti D., Hansen S. H., Vogelsberger M., 2018, MNRAS, 474, 746
Brown M. L., Taylor A. N., Hambly N. C., Dye S., 2002, MNRAS, 333, 501
Catelan P., Kamionkowski M., Blandford R. D., 2001, MNRAS, 320, L7
Chisari N. et al., 2015, MNRAS, 454, 2736
Chisari N. et al., 2016b, MNRAS, 461, 2702
Chisari N. E. et al., 2017, MNRAS, 472, 1163
Chisari N. E., Dvorkin C., 2013, J. Cosmol. Astropart. Phys., 2013, 029
Chisari N. E., Dvorkin C., Schmidt F., 2014, Phys. Rev. D, 90, 043527
Chisari N. E., Dvorkin C., Schmidt F., Spergel D. N., 2016a, Phys. Rev. D, 94, 123507
Codis S. et al., 2015, MNRAS, 448, 3391
Correa C. A., 2020, MNRAS, 503, 920

Crittenden R. G., Natarajan P., Pen U.-L., Theuns T., 2001, ApJ, 559, 552
Croft R. A. C., Metzler C. A., 2000, ApJ, 545, 561
Dalla Vecchia C., Schaye J., 2008, MNRAS, 387, 1431
Fortuna M. C., Hoekstra H., Joachimi B., Johnston H., Chisari N. E., Georgiou C., Mahony C., 2020, MNRAS, 501, 2983
Georgiou C. et al., 2019a, A&A, 622, A90
Georgiou C. et al., 2019b, A&A, 628, A31
Harvey D., Courbin F., Kneib J. P., McCarthy I. G., 2017, MNRAS, 472, 1972
Harvey D., Revaz Y., Robertson A., Hausammann L., 2018, MNRAS, 481, L89
Harvey D., Robertson A., Massey R., McCarthy I. G., 2019, MNRAS, 488, 1572
Heavens A., Refregier A., Heymans C., 2000, MNRAS, 319, 649
Heymans C., Brown M., Heavens A., Meisenheimer K., Taylor A., Wolf C., 2004, MNRAS, 347, 895
Heymans C., White M., Heavens A., Vale C., van Waerbeke L., 2006, MNRAS, 371, 750
Hilbert S., Xu D., Schneider P., Springel V., Vogelsberger M., Hernquist L., 2017, MNRAS, 468, 790
Hinshaw G. et al., 2013, ApJS, 208, 19
Hirata C. M., Seljak U., 2004, Phys. Rev. D, 70, 063526
Hirata C. M., Mandelbaum R., Ishak M., Seljak U., Nichol R., Pimbblet K. A., Ross N. P., Wake D., 2007, MNRAS, 381, 1197
Ivezić Ž. et al., 2019, ApJ, 873, 111
Joachimi B., Mandelbaum R., Abdalla F. B., Bridle S. L., 2011, A&A, 527, A26
Johnston H. et al., 2019, A&A, 624, A30
Kaplinghat M., Tulin S., Yu H.-B., 2016, Phys. Rev. Lett., 116, 041302
Kaplinghat M., Valli M., Yu H.-B., 2019, MNRAS, 490, 231
King L. J., 2005, A&A, 441, 47
Kirk D., Bridle S., Schneider M., 2010, MNRAS, 408, 1502
Kirk D., Rassat A., Host O., Bridle S., 2012, MNRAS, 424, 1647
Kraljic K., Davé R., Pichon C., 2020, MNRAS, 493, 362
Krause E., Eifler T., Blazek J., 2016, MNRAS, 456, 207
L'Huillier B., Winther H. A., Mota D. F., Park C., Kim J., 2017, MNRAS, 468, 3174
Laureijs R. et al., 2011, preprint (arXiv:1110.3193)
Lee J., Pen U.-L., 2000, ApJ, 532, L5
McCarthy I. G., Schaye J., Bird S., Le Brun A. M. C., 2017, MNRAS, 465, 2936
McCarthy I. G., Bird S., Schaye J., Harnois-Deraps J., Font A. S., van Waerbeke L., 2018, MNRAS, 476, 2999
Mackey J., White M., Kamionkowski M., 2002, MNRAS, 332, 788
Mandelbaum R., Hirata C. M., Ishak M., Seljak U., Brinkmann J., 2006, MNRAS, 367, 611
Newman A. B., Treu T., Ellis R. S., Sand D. J., Nipoti C., Richard J., Jullo E., 2013, ApJ, 765, 24

Okumura T., Jing Y. P., Li C., 2009, ApJ, 694, 214
Piras D., Joachimi B., Schäfer B. M., Bonamigo M., Hilbert S., van Uitert E., 2018, MNRAS, 474, 1165
Read J. I., Walker M. G., Steger P., 2018, MNRAS, 481, 860
Robertson A., Massey R., Eke V., Bower R., 2015, MNRAS, 453, 2267
Robertson A., Harvey D., Massey R., Eke V., McCarthy I. G., Jauzac M., Li B., Schaye J., 2019, MNRAS, 488, 3646
Sagunski L., Gad-Nasr S., Colquhoun B., Robertson A., Tulin S., 2021, J. Cosmol. Astropart. Phys., 2021, 024
Samuroff S., Mandelbaum R., Blazek J., 2020, preprint (arXiv:2009.10735)
Schaye J. et al., 2010, MNRAS, 402, 1536
Schaye J., Dalla Vecchia C., 2008, MNRAS, 383, 1210
Schmidt F., Chisari N. E., Dvorkin C., 2015, J. Cosmol. Astropart. Phys., 2015, 032
Schneider M. D., Bridle S., 2010, MNRAS, 402, 2127
Shi J., Kurita T., Takada M., Osato K., Kobayashi Y., Nishimichi T., 2020, preprint (arXiv:2009.00276)
Singh S., Mandelbaum R., 2016, MNRAS, 457, 2301
Singh S., Mandelbaum R., More S., 2015, MNRAS, 450, 2195
Soussana A. et al., 2020, MNRAS, 492, 4268
Springel V., 2005, MNRAS, 364, 1105
Springel V., White S. D. M., Tormen G., Kauffmann G., 2001, MNRAS, 328, 726
Tenneti A., Singh S., Mandelbaum R., di Matteo T., Feng Y., Khandai N., 2015a, MNRAS, 448, 3522
Tenneti A., Mandelbaum R., Di Matteo T., Kiessling A., Khandai N., 2015b, MNRAS, 453, 469
Tulin S., Yu H.-B., 2017, Phys. Rep., 730, 1
van Daalen M. P., Schaye J., McCarthy I. G., Booth C. M., Dalla Vecchia C., 2014, MNRAS, 440, 2997
van Uitert E., Joachimi B., 2017, MNRAS, 468, 4502
Velliscig M. et al., 2015, MNRAS, 454, 3328
Vlah Z., Chisari N. E., Schmidt F., 2020a, J. Cosmol. Astropart. Phys., 2020, 025
Vlah Z., Chisari N. E., Schmidt F., 2020b, J. Cosmol. Astropart. Phys., 2020, 025
Wiersma R. P. C., Schaye J., Smith B. D., 2009a, MNRAS, 393, 99
Wiersma R. P. C., Schaye J., Theuns T., Dalla Vecchia C., Tornatore L., 2009b, MNRAS, 399, 574

APPENDIX A: REDSHIFT EVOLUTION OF GALAXY CLUSTERING

Our results from Section 4.2 suggest that the alignment signal, w_{g+}, of the most massive 4800 central galaxies in our simulations increases with redshift up to $z = 0.375$. In this section, we verify that the clustering of those galaxies *decreases* with increasing redshift, as
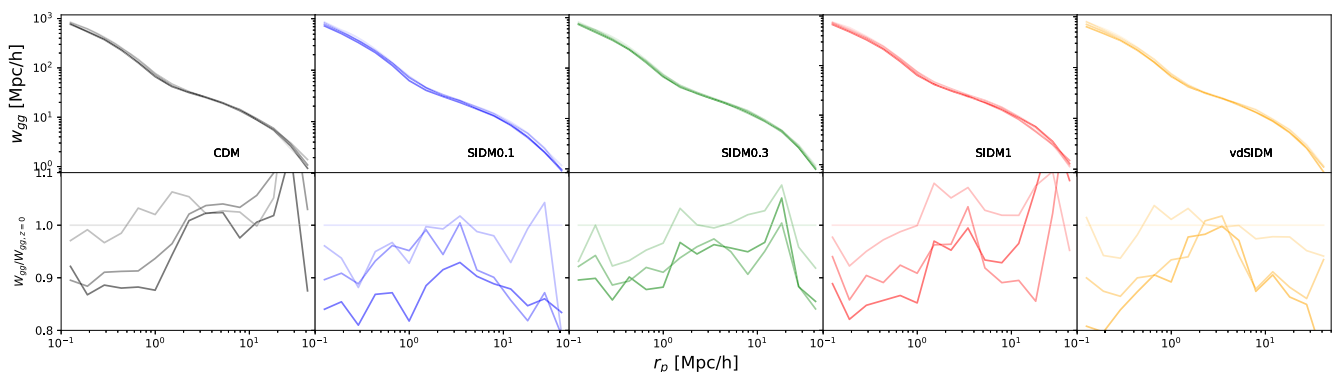
Figure A1. The top panel shows the projected clustering statistics for the 4800 most massive galaxies in the simulations for each dark matter model (left- to right-hand side). The bottom panels show the ratios of the clustering signal at a given redshift with respect to the $z = 0$ case. Increasing redshifts, up to $z = 0.375$, correspond to darker colours. The clustering signal is suppressed at higher redshifts for all models, as expected for a number selected sample.

expected for a sample where the number of galaxies is preserved across redshift bins.

The results are shown in Fig. A1, where each panel from the left- to right-hand side corresponds to a different dark matter model. The bottom panels show the ratio of the clustering signal at a given redshift compared to the $z = 0$ case. Darker curves indicate higher redshifts. We observe that indeed the clustering of the galaxies is consistently higher at lower redshift for all models. This is expected from our selection: The N most massive galaxies at $z = 0$ are expected to be more highly biased than the N most massive galaxies at a higher redshift. This is in contrast to the redshift evolution of the alignments of such sample, shown in Fig. 6, where we observed that alignments, as measured via w_{g+}, increased with increasing redshift. Our results here allow us to factor out the decreasing clustering evolution and reinforce the conclusion that the alignment of our sample increases towards higher redshifts.

This paper has been typeset from a TEX/LATEX file prepared by the author.